Energetics of isolated and stormtime substorms

N. Østgaard[1]

Department of Physics, University of Oslo, Norway

E. Tanskanen[2]

Finnish Meteorological Institute, Helsinki, Finland

A fundamental question in the physics of solar-magnetospheric-ionospheric (SMI) interaction is to understand how the solar wind energy is transferred, stored and distributed in the magnetospheric-ionospheric (MI) system. In this paper we discuss how well parameterized expressions can estimate the energy sources and sinks in the SMI system. We also present some recent results from two energy budget studies. We find that the overall energy coupling efficiency, defined as the ratio of energy dissipated in the MI system to the total available solar wind kinetic energy (U_{SW}) is <1%. We also find that the Akasofu ϵ-parameter, which approximates the solar wind input due to day-side reconnection, does not always provides enough energy to balance the energy sinks in the MI system. Allowing for viscous interaction between the solar wind and the magnetosphere, such a mechanism only need to transfer 0.17% of U_{SW} to balance the energy budget. The dominant energy sink in the MI system is found to be the U_J during both isolated and stormtime substorms. The particle precipitation energy flux (U_A) is about 1/2 of U_J. Several studies indicate that U_R is about the same as U_A even during magnetic storms. Isolated substorms are found to be five times as numerous, but half as intense as stormtime substorms. However, over a 2-year period twice as much energy is dissipated during isolated substorms than during stormtime substorms, indicating that isolated substorms are the main process by which solar wind energy is dissipated in the MI energy sinks.

[1] Now at Space Sciences Laboratory, University of California, Berkeley, California

[2] Now at Goddard Space Flight Center, Greenbelt, Maryland

The Storm-Substorm Relationship
Geophysical Monograph ??

1. INTRODUCTION

One of the fundamental questions in the physics of solar-magnetospheric-ionospheric (SMI) interaction is to understand and to quantify how the flow of energy from the Sun carried by the solar wind is transferred, stored and distributed in the magnetospheric-ionospheric (MI) system during magnetically disturbed conditions like substorms, convection events and magnetic storms. The growing interest of space weather activities during the last few years has further emphasized the importance of energy budget studies of the SMI system during different levels of magnetic disturbances. It is fairly well accepted that the solar wind, carrying the interplanetary magnetic field (IMF), can penetrate the magnetic shielding of the Earth through a reconnection process on the day-side magnetopause and thereby transfer energy and momentum into the magnetosphere, although other mechanisms of energy transfer as viscous interaction between the solar wind and the magnetosphere may be important during specific magnetic conditions. The transferred energy can then either be deposited "directly" into the ionosphere with a typical delay of ~20 min or be stored in the magnetosphere and with a typical delay time of ~60 min be dissipated during substorms [Bargatze et al., 1985; Tsurutani et al., 1985; Liou et al., 1998]. These two categories of energy deposition events are usually referred to as directly driven events and loading-unloading events [Baker et al., 1984; Rostoker, 1991; Elphinstone et al., 1996]. The directly (solar wind) driven processes indicate convection activity that is formed as an immediate response to the enhanced energy input [Baker et al., 1997]. The loading-unloading events refer to the storing of magnetic and kinetic energy in the magnetosphere during growth phase and the abrupt substorm breakup with the subsequent global expansion of the auroral oval. The main part of the energy needed to build up substorms is gained during substorm expansion and recovery phases, whereas the growth phase is needed for pre-conditioning the magnetotail to allow the global instability to grow [Kallio et al., 2000]. Magnetospheric substorms and magnetic storms are the main processes by which the solar wind energy is carried to the MI energy sinks. Magnetic storms may include both substorms and convection events and it has been suggested that there are fundamental differences between substorms occurring at storm and non-storm times [Baumjohann et al., 1996].

The purpose of this paper is two-fold. First, in Section 2, we give a tutorial presentation of the most impor-

tant sources and sinks of energy in the SMI system and how well we can quantify these different energy forms. Secondly, in Sections 3 and 4, we present some recent results from energy budget studies during isolated and stormtime substorms. One study utilizes the imaging instruments on board the Polar satellite to obtain an estimate of the energy flux of precipitating electrons from 0.1 to 100 keV and examines the total energy budget for 7 isolated substorms [Østgaard et al., 2002 A, in press]. Another study focuses on the Joule dissipation for isolated and stormtime substorms, separately, from 1997 and 1999, and gives statistical results in terms of solar wind input, Joule dissipation, intensity, duration, occurrence frequency and time of onset [Tanskanen et al., 2002].

2. ENERGY SOURCES AND SINKS IN THE SMI SYSTEM

The main source of energy for the MI system is the solar wind, although the conductance increase due to solar radiation must be considered when the Joule heating of ionosphere is estimated. The three most important forms of ionospheric and magnetospheric energy dissipation rates are the energy increase of the ring current (U_R), the Joule heating rate of the atmosphere (U_J) and the energy flux by particle precipitation (U_A) [Akasofu, 1981; Weiss et al., 1992; Baker et al., 1997; Knipp et al., 1998], although other forms of energy dissipation like the plasma sheet heating, the energy returned to the solar wind by plasmoid ejections from the tail and the production of relativistic electrons might be considered as well [Baker et al., 1997; Lu et al., 1998; Ieda et al., 1998].

2.1. The solar wind energy source

To quantify the energy transfer from the solar wind into the magnetosphere Perrault and Akasofu [1978] and Akasofu [1981] examined magnetic storms and substorms to estimate the different forms of ionospheric and magnetospheric energy dissipation. By using the Dst index to estimate U_R and the auroral electrojet index AE to estimate U_J and U_A in both hemispheres they obtained an estimate of the total energy dissipation rate in the MI system, $U_T = U_R + U_J + U_A$. By comparing U_T with the solar wind parameters they derived the Akasofu's energy input parameter ϵ [Akasofu, 1981], here given in SI units,

$$\epsilon[\mathrm{W}] = 10^7 v B^2 \sin^4(\frac{\theta_c}{2}) l_0^2 \qquad (1)$$

where v is the solar wind bulk speed, B is the magnitude of the interplanetary magnetic field and θ_c is the clock angle of the IMF which is defined as the polar angle between the IMF as projected into the Y-Z plane and the Z-axis in GSM coordinates. The parameter l_0 is an empirically determined scale length, sometimes interpreted in terms of the merging region at the sub-solar magnetopause, assumed to be 7 R_E. The ϵ-parameter is a semi-empirical function which has been shown to approximate the solar wind energy input to the magnetosphere due to day-side reconnection. Because of its θ_c dependence ϵ maximizes when IMF turns southward and approaches zero for northward IMF. Efforts have been made to find other energy transfer parameters that would give better correlation with auroral measurements [Holzer and Slavin, 1982; Gonzalez et al., 1994; Liou et al., 1998; Stamper et al., 1999] but they have not provided more accurate estimates of the magnitude of the energy transfer.

The ϵ-parameter is frequently used and many studies show that during mainly southward IMF conditions the parameter gives a reasonable estimate of the total energy transferred into the magnetosphere [Zwickl et al., 1987; Baker et al., 1997; Lu et al., 1998; Liou et al., 1998]. However, by studying time intervals of intense northward IMF events that last for several hours some studies [e.g., Tsurutani and Gonzalez, 1995] have found there is still energy dissipated in the MI system. As the energy transfer due to reconnection during such IMF conditions cannot balance the energy sinks in the MI system, a viscous type of interaction between the solar wind and the magnetosphere has been suggested as an additional energy transfer mechanism. This was first suggested by Axford and Hines [1961] and has later been supported by energy budget studies [Tsurutani and Gonzalez, 1995; Lu et al., 1998; Knipp et al., 1998; Østgaard et al., 2002 A, in press]. As the physical meaning of viscous interaction in a collisionless plasma is not obvious [Parks, 1991] some kind of wave-particle interaction has been suggested to be the coupling mechanism. Farrugia et al. [2001] argue that the Kelvin-Helmholtz instability is the major contributor to viscous coupling, a mechanism that is most efficient during northward IMF conditions. The energy transferred by viscous interaction (U_{VI}) can be expressed as a fraction, σ_v, of the total available kinetic energy of the solar wind (Eq. 2).

$$U_{VI} = \sigma_v U_{SW} = \sigma_v \cdot 1/2 \rho v^3 A \qquad (2)$$

where ρ is the solar wind mass density (including the Helium content in the solar wind), v is the solar wind

radial speed and A is the magnetopause cross section. An estimate of A is given by Shue et al. [1997, 1998] who found that A depends on the solar wind dynamic pressure and the IMF B_Z value. The overall coupling efficiency of the solar wind kinetic power to the magnetosphere is thought to be ~1% [Stern, 1984].

2.2. Ring current

During magnetically disturbed conditions particle injections in the tail will lead to an intensification of the ring current, which can be monitored as geomagnetic disturbances at low latitudes. Four stations near the equator have therefore been selected to provide a global index (Dst) for the ring current [Sugiura, 1964]. Variations in the solar wind pressure modulate currents flowing at the day-side magnetopause [Gonzalez et al., 1994] and lead to a compression of the magnetosphere; this will be observed as an increase in the Dst index. As this effect is not related to the ring current, the Dst index is corrected for this solar pressure effect. An expression for the pressure corrected Dst^* is given by Gonzalez et al. [1994].

$$Dst^*[nT] = Dst - 5 \cdot 10^5 [\frac{nT}{(Jm^{-3})^{1/2}}] p^{1/2} - 20[nT] \quad (3)$$

where p is the solar wind dynamic pressure. Using the corrected Dst^* index as input, the following equation has been found to give a good estimate of the ring current energy change, U_R [Perrault and Akasofu, 1978; Akasofu, 1981; Zwickl et al., 1987; Gonzalez et al., 1994],

$$U_R[\mathrm{GW}] = 4 \cdot 10^4 (\frac{\partial Dst^*}{\partial t} + \frac{Dst^*}{\tau}) \quad (4)$$

where Dst^* is expressed in nT and τ is the ring current lifetime given in seconds. Many studies have used the scaling factor, $4 \cdot 10^4$ [Baker et al., 1997; Lu et al., 1998], which is derived under the assumption of a symmetric ring current in a dipole magnetic field [Akasofu, 1981], while Prigancova and Feldstein [1992] used a slightly lower value $2.7 \cdot 10^4$. The value from [Akasofu, 1981] may be considered as an upper bound as the effect of an asymmetric ring current should imply a lower estimate of U_R for the same amplitude of Dst. The ring current lifetime, τ, which depends on loss processes mainly due to charge exchange between ring current ions and exospheric neutrals, is not thought to be constant, but is strongly dependent on the amplitude of Dst^*. The magnitude of U_R is consequently very sensitive to the choice of τ [Zwickl et al., 1987; Prigancova and Feldstein, 1992], especially for large amplitudes of Dst during the main phase of magnetic storms [Gonzalez et al.,

1994; Valdivia et al., 1996]. Lu et al. [1998] makes a reasonable compromise between the various differentiated τ values presented by Akasofu [1981], Prigancova and Feldstein [1992] and Gonzalez et al. [1994]. Based on nonlinear dynamical methods Vassiliadis et al. [1999] report τ values similar but less differentiated than the values used by Lu et al. [1998]. They also argue that a smaller τ should be applied for small magnetic storms.

2.3. Joule heating

The Joule heating is controlled by the Pedersen currents and the electric field, which are linked by the Pedersen conductance. As none of these quantities can be monitored directly on a global scale different methods have been developed to estimate at least two of them remotely. Based on radar measurements [Ahn et al., 1983; Ahn et al., 1989], magnetic measurements [Baumjohann and Kamide, 1984] or huge data sets as input to the assimilative mapping of ionospheric electrodynamics (AMIE) procedure [Richmond, 1990; Cooper et al., 1995; Lu et al., 1995; Lu et al., 1998], the global Joule heating has been found to be closely related to the AE index. It is widely known that the auroral electrojet indices show seasonal variations [Russell and McPherron, 1973; Allen and Kroehl, 1975; Kamide and Akasofu, 1983], such that the activity maximizes near equinox and is lower during solstice. Some studies have examined these variations to establish a more accurate relation between U_J and the geomagnetic indices [Nisbet, 1982; Lu et al., 1998]. However, most of the relations do not take into account either the neutral wind effect or variations of the large scale electric field, which both can affect the estimate of U_J significantly [Lu et al., 1995; Emery et al., 1999]. A more thorough discussion about the different effects important for calculating the U_J and an evaluation of the different parameterized relations between U_J and AE is given by Østgaard et al. [2002 A, in press]. A common limitation using global indices to estimate U_J is that local effects are not properly considered.

As the global indices (i.e., AE and AL) do not always reflect the maximum disturbance due to the ionospheric currents, local indices in limited local time sectors, such as CU and CL from the CANOPUS chain [Rostoker et al., 1995] or the IU and IL indices from the IMAGE chain [Kallio et al., 2000; Tanskanen et al., 2002] have been found to give more accurate representation for geomagnetic activity [Kauristie et al., 1996] due to their extended latitudinal coverage. Kauristie et al. [1996] found that westward electrojet index from the IMAGE chain catches at least 70% of the AL activity during pe-

riod 1800 - 0400 UT (2030 - 0630 MLT). Especially in the middle of this optimal UT-sector, the IL index usually show stronger activity than the AL index. However, it is true that between 1600 - 1800 UT (1830 and 2030 MLT) the IMAGE chain can underestimate substorm intensity, because of its limited longitudinal coverage.

2.4. Auroral particle precipitation

As particle precipitation through ionization affects the Hall conductance and thereby increases the Hall currents resulting in disturbances of the geomagnetic field, U_A is believed to be related to the AE (or AL) indices [Akasofu, 1981; Spiro et al., 1982; Ahn et al., 1983; Richmond, 1990; Lu et al., 1998; Østgaard et al., 2002 B, in press]. Where instantaneous global measurements of electron precipitation are not available, U_A can be derived indirectly from radars or magnetic data or from statistical particle measurements by low-altitude satellites. Østgaard et al. [2002 B, in press] used X-ray and UV emissions to derive U_A from 0.1 to 100 keV. By comparing this result with the parameterized methods based on AE or AL they found that most of these methods underestimate U_A significantly. This may be due to the fact that most of these parameterized methods are developed by using data that only cover electron energies up to 20-30 keV. To examine how much the energetic electrons (> 20 keV) contribute to the total U_A Østgaard et al. [2002 A, in press] calculated how much of the U_A derived from UVI and PIXIE that would be estimated if only the UVI is used. The UVI instrument is most sensitive to electrons $< 20 - 30$ keV, while the PIXIE instrument is sensitive to electrons up to $\sim$100 keV. It was found that during growth phase the U_A derived from UV emissions only, gives about 90 - 100% of the total U_A, while the fraction gets closer to 80% during the recovery phase. The energy contribution from the hard tail in the electron spectrum was consequently found to be no more than 20-30% on a global scale and could not explain why some of the parameterized methods only provide 30% of the U_A [Østgaard et al., 2002 B, in press]. Comparing the electron energy flux derived at different local times the fraction was about 90-100% in the day, dusk and midnight sector and closer to 80% in the dawn sector. These results are consistent with the existence of hard electron spectra in the post-midnight to dawn sector and during the recovery phase of substorms. However, for physical processes like Hall conductance increases, cosmic radio wave absorption or wave-particle interaction this tail is the most important part of the energy spectrum.

2.5. Other energy sinks

There are other energy sinks in the MI system that are not so straightforward to estimate. In a statistical study of plasmoids Ieda et al. [1998] found that on average 1.8 plasmoids were ejected down the tail during substorms and that the energy released by plasmoids was estimated to be roughly 10^{15} J in the course of a substorm. During a magnetic cloud event Lu et al. [1998] suggested the plasma sheet heating to be roughly $\sim$100 GW [Weiss et al., 1992] and in the same range as the U_A. They also examined the SAMPEX data from the Polar satellite of MeV electrons and found the energy flux of relativistic electrons to be about 0.5 GW during the event. Baker et al. [2001] have examined relativistic electron data from several spacecraft over a 7-year period and found that a rather steady 1% of the solar wind energy transfer estimated by ϵ is converted to relativistic electron energy. Other minor energy sinks are auroral kilo-metric radiation and ultra-low frequency (ULF) magnetic field oscillations which account for $\leq$1% of the magnetospheric dissipation [Baker et al., 1997].

2.6. Energy budget studies

A general understanding of the energy flow from the solar wind to the MI system is given by Stern [1984]. Magnetic storm and substorm energetics have been studied since the beginning of the 1980's when the role of ring current was thought to be overwhelming relatively to other energy sinks [Akasofu, 1981]. Since then several studies have found that during both substorms and magnetic storms the ionospheric energy sinks are dominant [Weiss et al., 1992; Lu et al., 1998; Knipp et al., 1998; Tanskanen et al., 2002; Turner et al., 2001, in press; Østgaard et al., 2002 A, in press]. Weiss et al. [1992] concluded that both statistical and case studies indicate that the predominant energy dissipation mechanism is the Joule heating. Gonzalez et al. [1994] have questioned this result due to the ring current decay time Weiss et al. [1992] used and claimed that U_R is still the dominant energy sink during magnetic storms.

Examining a severe magnetic storm 2-11 November, 1993, Knipp et al. [1998] utilized a huge database to estimate both $\epsilon, U_{SW}, U_R, U_J$ and U_A and presented a total energy budget for the entire storm period. As they used the ring current decay time suggested by Akasofu [1981] their U_R values are probably overestimated rather than underestimated. Only at the very onset of the storm U_R was found to be the dominant energy sink. After 12 hours U_J was found to be the dominant energy sink (55%) and for the entire 10-day period of

the storm they found the energy to be distributed by 60%, 23% and 17% to U_J, U_A and U_R, respectively. Lu et al. [1998] used a comprehensive set of data to study the total energy budget for the magnetic cloud event on January 10-11, 1997. They used the AMIE procedure supported by auroral electron energy fluxes derived from ultraviolet (UV) images to estimate U_J and U_A. Comparing average energy dissipation they found the energy to be distributed 47.5% to U_J and 30%, 22.5% to U_R and U_A, respectively.

Other studies have focused on more specific aspects of the ionospheric energy dissipation. Lu et al. [1995] used the National Center for Atmospheric Research Thermosphere-Ionosphere General Circulation Model (NCAR TIGCM) and the AMIE procedure to examine the effect of neutral winds on the U_J during the Geospace Environment Modeling (GEM) campaign period of March 28-29, 1992. They also calculated the ratio U_J/U_A during that period. Emery et al. [1999] examined the same storm period as studied earlier by Knipp et al. [1998] to determine the thermospheric neutral response to the magnetic storm. Using the TIGCM and AMIE procedures they estimated the neutral wind effect on the U_J, the seasonal variations of U_J as well as the ratio U_J/U_A. Liou et al. [1998] used the UV images from Polar to estimate the energy deposition by precipitation. Kallio et al. [2000] used the IL index from the International Monitor for Auroral Geomagnetic Effects (IMAGE) as input to the relation found by Ahn et al. [1983] to present statistical results of the U_J during isolated substorms compared with the solar wind input estimated by the ϵ-parameter.

3. TOTAL ENERGY BUDGET FOR 7 SUBSTORMS

In this section we will present results from a study where the imagery on board the Polar satellite were utilized to obtain a more accurate estimate of the U_A and where the energy sources and sinks during 7 isolated substorms during 1997 were examined in detail (see Østgaard et al. [2002 A, in press] for a more detailed description of these results). Although the solar wind conditions for the 7 substorms diversed, none of the substorms occurred during large magnetic storms, see Table 1.

Table 1

Solar wind density and velocity data from the solar wind experiment [Ogilvie et al., 1995] and IMF measurements by the magnetic field experiment [Lepping et al., 1995] on board the WIND spacecraft were used to estimate the solar wind input due to day-side recon-

nection (ϵ, Eq. 1) and the total available kinetic energy (U_{SW}, Eq. 2).

To estimate the increase of the ring current the pressure corrected Dst^* (Eq. 3) was used as input for Eq. 4 with the differentiated ring current life time (τ) values recommended by Lu et al. [1998]. Our choice of τ should be reasonable as none of the substorms occurred during large magnetic storms with large amplitudes of Dst^*. As we used the constant, $4 \cdot 10^4$ [Akasofu, 1981], derived under the assumption of an asymmetric ring current the U_R values might be slightly overestimated.

The different parameterized methods to obtain U_J estimates based on the AE index were reviewed to see how seasonal and hemispherical effects as well as the number of stations that were used to calculate the auroral electrojet indices could properly be taken into account. The quick look AE_{QL}, AU_{QL} and AL_{QL} indices, at 1 min resolution were obtained from the World Data Center for Geomagnetism, in Kyoto, Japan. During the examined events these indices were based on 6-8 of the 12 standard stations, except for one event (July 31, 1997) where only 4 stations were included. The advantage of choosing the quick look auroral electrojet indices is that they are easily accessible, but it requires that one must make certain that the few stations are well located with regard to the regions of intense electron precipitation. Based on these considerations it was found that U_J in both hemispheres for these substorms during summer time conditions could be estimated by Eq. 5 [Østgaard et al., 2002 A, in press].

$$U_J[\mathrm{GW}] = 0.54AE + 1.8 \qquad (5)$$

The neutral wind effect and the variations of the large scale electric field were not taken into account. Lu et al. [1995] and Emery et al. [1999] found that U_J would be decreased by 10-30% if a complete calculation of U_J including the neutral wind mechanical energy increase, U_{NW}, would be carried out. Codrescu et al. [1995] and Lu et al. [1998] found that if realistic electric field variability is taking into account, the U_J estimate would be increased by 10-30%. As these two effects are in the same range and opposite, they may cancel, but these considerations also indicate that the U_J value we use is somewhat uncertain.

To estimate the auroral energy dissipation by particle precipitation, U_A, the combined measurements from the Polar Ionospheric X-ray Imaging Experiment (PIXIE) [Imhof et al., 1995] and the Ultraviolet Imager (UVI) [Torr et al., 1995] were utilized. From these two imagers it is possible to derive 5 min-averages of $U_{A,north}$ in the 0.1-100 keV energy interval. A description on

how a four-parameter electron spectra can be derived from PIXIE measurements is given by Østgaard et al. [2000, 2001] and a description of the technique used to derive a two-parameter electron spectrum from the UVI measurements is given by Germany et al. [1997, 1998a, b]. A validation of combining the two measurements and techniques by comparing with directly measured electron spectra by low-altitude satellites is given by Østgaard et al. [2001] . The U_A in both hemispheres was calculated by multiplying the $U_{A,north}$ by a factor 2. This is consistent with the results from Lu et al. [1998]; using the AMIE procedure supported with UVI data they found that the energy deposition rates in the two hemispheres were almost similar.

Several criteria had to be met which made the number of available substorms for this study limited. We required that the PIXIE instrument should be fully operating to provide measurements in all energy bands during the entire substorm including both the directly driven growth phase and the loading-unloading substorm. As UVI field of view is sometimes too small to cover the entire global substorm only substorms occurring when Polar was close to apogee could be examined. During 1997, seven substorms were found to meet these criteria.

To present the method of analysis we show in Figure 1 the substorms that occurred on July 24, 1997. Panels a-d show the solar wind parameters and Panels e-f show the ϵ-parameter and U_{SW} derived from these parameters. Panel g-i show the three energy sinks, U_R, U_J and U_A and Panel j shows the AE index. The solar wind data is shifted in time due to the radial distance of the WIND spacecraft relative to the subsolar point of the magnetopause. We have also added 5 min to account for the propagation time for a disturbance in the solar wind to affect the inner magnetosphere and thereby be observable in the ionosphere and on the ground [Kan et al., 1991]. The results from Collier et al. [1998] have been used to estimate the uncertainty of the time shift. The location of the WIND spacecraft, the time shift and the uncertainty of this time shift are indicated in Panel c. To examine the energy budget the time-integrated values of ϵ and U_{SW} as well as the energy deposition in the MI system were calculated. In order to include the energy that was transferred into the magnetosphere prior to and during the substorms, the AE index was examined to find a quiet period before the substorm. This time, t_1, was taken to be the beginning of the growth phase. For all the events this time was found to correspond fairly well with the increase in the ϵ-parameter, indicating that the time shifts of the solar wind data

Figure 1

are reasonable. The end of integration time, t_2, was determined by the end of PIXIE and UVI data. For the different forms of energy the time-integrated value $W(U_X)$ from t_1 to t_2

$$W(U_X)[J] = \int_{t_1}^{t_2} U_X(t)dt \qquad (6)$$

is calculated (see Panel e-i).

In Table 2 (from Østgaard et al. [2002 A, in press]) the time-integrated energy sinks and sources in the SMI system, are listed for all the 7 substorms that occurred during the 4 days in 1997. For $W(U_R), W(U_J)$ and $W(U_A)$ the fractions (in %) of the total energy dissipation ($W(U_T) = W(U_R) + W(U_J) + W(U_A)$) are calculated. Notice that the time of integration is shorter for $W(U_A)$ than for the other energies due to the limited operation time of the imagers on Polar, giving a slight underestimate of $W(U_A)$.

Table 2

4. STATISTICAL RESULTS FOR ISOLATED AND STORMTIME SUBSTORMS

In this section we present statistical results on isolated and stormtime substorms in terms of solar wind input, Joule dissipation, intensity, duration, occurrence frequency and time of onset (for a more detailed description of these results see Tanskanen et al. [2002]). We have examined 839 substorm events in order to study the substorm energy budget. Isolated (IS) and stormtime (SS) substorms were analyzed separately using time integrals of energy input and Joule dissipation as described in the following subsection. A substorm was termed isolated if the Dst index was above –40 nT, otherwise the event was classified as a stormtime substorm.

4.1. Data set and method description

The data set covers two years of IMAGE ground-based magnetic observations at 60-s resolution, combined with simultaneous WIND and ACE solar wind and IMF observations. All substorms during 1997 and 1999 in the time sector 16–02 UT (1830 - 0430 MLT) were analyzed. During this local time period IMAGE is near the midnight sector, which is the best location to record substorm activity [Akasofu, 1964; Caan et al., 1978]. Solar wind magnetic field was measured using WIND Magnetic Field Instrument (60-s time resolution) [Lepping et al., 1995] for 1997 and ACE Magnetic Field Experiment (16-s time resolution) [Smith et al., 1998] for 1999. Plasma velocities were taken from WIND Solar Wind Experiment (92-s time resolution) [Ogilvie et al., 1995]

for 1997 and from ACE Solar Wind Electron Proton Alpha Monitor (64-s time resolution) [McComas et al., 1998] for 1999. The IL index [Kallio et al., 2000], a proxy of westward electrojet index AL, is constructed from 16 (22) magnetometers of the IMAGE magnetometer array [Syrjäsuo et al., 1998] for 1997 (1999) (for more details see Tanskanen et al. [2002]). Due to its extended latitudinal coverage, the IL index correctly records the occurrence and intensity of substorms both at high and low latitudes, in addition to the typical auroral latitudes. According to Kauristie et al. [1996] the maximum electrojet activity derived from the IMAGE chain is equal to or larger than the AL index within the local time sector considered in our study.

In selecting substorm events, a minimum IL intensity of $\mid IL \mid = 100$ nT was used to avoid ambiguous identification during very low-level activity conditions. The magnetospheric energy input, $W(\epsilon)$, was computed by integrating the ϵ parameter (Eq. 1) as

$$W(\epsilon) = \int \epsilon \, dt. \tag{7}$$

Time integration of the ϵ parameter was started from the beginning of the substorm, defined from the southward turning of $IMF\ B_Z$, and it was continued until the end of the substorm when the IL index returned to near zero. The ϵs parameter was evaluated at the subsolar magnetopause, obtained by shifting the solar wind time series from the upstream solar wind to the magnetopause at 10 R_E by $\Delta t = \Delta x/v$, where v is the average speed observed around the substorm onset time. Similar time integral for the IL index was used to compute the two-hemisphere Joule dissipation

$$W(U_J) = 2 \int aIL \, dt \tag{8}$$

during the substorm event, where a is a conversion factor from IL in [nT] to power. We have used the conversion factor $a = 3 \cdot 10^8$ given by Ahn et al. [1983]. As these substorms occurred during different seasons we have simply multiplied the northern hemispherical value by a factor 2 to get the $W(U_J)$ for both hemispheres. This is slightly different from Eq 5 used for the 7 substorms, where the seasonal effects were taken into account [Østgaard et al., 2002 A, in press].

4.2. Number, intensity and frequency of events

In total, 698 (83%) of the substorms in our data set were isolated with *Dst* above –40 nT (termed IS for isolated substorms). The intensities of isolated events,

as measured by the minimum of the IL index, ranged from –100 nT to –1700 nT, the average being –347 nT. Stormtime substorms (SS) were twice as intense as isolated substorms, but the minimum was around –1700 nT. Thus, there seems to be an upper limit for substorm intensity, which is independent of the simultaneous ring current activity. On the other hand, it seems that the upper limit for the substorm intensity depends on the solar cycle phase, being –1400 nT for the more quiet year 1997 and –1700 nT for 1999 close to solar maximum. Intensity histograms for ISs and SSs, binned every 100 nT, are shown in Figure 2.

Figure 2

Frequency of isolated (stormtime) substorms was computed by dividing the total number of events, n_{IS} (n_{SS}), by the total time during the two years under study when Dst was above and equal to or below –40 nT (T_{IS} and T_{SS}, respectively). Keep in mind that the total time periods are different for different types of events; 7106h for isolated and 563h for stormtime substorms.

$$f_{IS} = \frac{n_{IS}}{T_{IS}} = \frac{698}{7106h} = 0.1h^{-1}$$
$$f_{SS} = \frac{n_{SS}}{T_{SS}} = \frac{141}{563h} = 0.25h^{-1} \quad (9)$$

4.3. Input-Joule heating analysis

Total magnetospheric energy input, $W(\epsilon)$, and the two-hemisphere Joule dissipation, $W(U_J)$, are illustrated in Figure 3. Energy input and Joule dissipation histograms are shown in the vertical axis, and the number of events in the horizontal axis. Histograms for isolated substorms, binned by every $0.5 \cdot 10^{15}$ J, are shown in the left panel, and histograms for stormtime substorms, binned by every 10^{15} J, are shown in the right panel. The typical value of energy input, $W(\epsilon)$, is $0.1 \cdot 10^{16}$ J for IS while it is $0.3 \cdot 10^{16}$ J for SS, and the histogram shows a much longer tail of $W(\epsilon)$ for SS. For the output, $W(U_J)$, most events occur in the lowest bin, $< 0.1 \cdot 10^{16}$ J, for IS, while there is a maximum at $0.2 \cdot 10^{16}$ J for SS. The ISs are five times as numerous, but only half as energetic as the SSs. The energy input varied from values below 10^{14} J to values larger than $6 \cdot 10^{15}$ J, the median being $1.4 \cdot 10^{15}$ J for IS and $3.5 \cdot 10^{15}$ J for SS. Both input distributions have long tails, with a total of ten events having $W(\epsilon)$ larger than $2 \cdot 10^{16}$ J.

Figure 3

The role of U_J in the total energy budget was further analyzed by computing ratios $W(U_J)/W(\epsilon)$ for each event in our data set. Figure 4 shows these ratios in

Figure 4

a histogram format, separately for IS and SS. $W(U_J)$ seems to account for typically (median) more than half of the input, over 60% for IS and about 50% for SS (Table 3). Averages showed even larger ratios for both classes of events (80% and 61%, respectively).

Table 3

Although single IS on average dissipates less energy than single SS, the yearly $W(U_J)$ during the isolated events exceeds the yearly $W(U_J)$ during stormtime substorms, because ISs are five times more numerous than SSs. Yearly $W(U_J)$ is computed by multiplying the number of events with the average Joule dissipation. In 1997 the yearly $W(U_J)$ through isolated substorms was $2.8 \cdot 10^{17}$ J and in 1999 about $5.0 \cdot 10^{17}$ J. Yearly stormtime $W(U_J)$ was $1.7 \cdot 10^{17}$ J during both years.

We have also examined the duration and the local time of the onset of ISs and SSs. We define the duration of the substorm, Δt, as the time period between the beginning of the substorm growth phase and the end of the recovery phase. The mean duration of all events in our database was 3 hours 50 minutes of which the growth phase took about 60 minutes. Isolated and stormtime substorm did not show large differences in duration (see Table 4). The average local time of onset for ISs was found to be ~2300 MLT. For stormtime substorms the local time of onset was 45 min earlier (~2215 MLT). Table 4 summarizes these results for the entire data set separately for IS and SS.

Table 4

5. DISCUSSION

5.1. Total energy budget for 7 substorms

As seen from Table 2, the time integrated total energy dissipation ($W(U_T)$) is distributed as 15%, 56% and 29% to $W(U_R), W(U_J)$ and $W(U_A)$, respectively, which is very close to what Knipp et al. [1998] found for the entire 10 days of the magnetic storm period of November, 1993 (17%, 60%, 23%). The main difference seems to be that our U_A is larger than in their study. In the rightmost column of Table 2 we have listed the coupling efficiency, expressed by the ratio $W(U_T)/W(U_{SW})$. The coupling efficiency ranges from 0.3 to 0.8%, which is in reasonable agreement with the 1% that according to Stern [1984] is the widely cited order of magnitude estimate of the energy extracted from the solar wind. The higher coupling efficiency found by Knipp et al. [1998] (6.9%) and Lu et al. [1995] (1.5%) can be explained by the different estimates of the magnetospheric cross section they used. We use the cross section suggested by Shue et al. [1997], which depends on the solar wind pressure and $IMF\ B_Z$ and is usually $\pi \cdot 10^2 \mathrm{R}_\mathrm{E}^2$. Knipp et al. [1998] used $7^2 \mathrm{R}_\mathrm{E}^2$ and Lu et al.

[1995] used $15^2 R_E^2$. Using the same cross section as we do, their coupling efficiencies would both become 1.1%.

Although none of the substorms occurred during large magnetic storms, the largest value of $W(U_R)$ (26%) on August 28 might be classified as a minor magnetic storm (-48 nT). However, we find that the average of 15% is still similar to the substorms on July 24 where the $W(U_R)$ is fairly small. It should also be noticed that the U_R might has been overestimated by using the scaling factor $(4 \cdot 10^4)$ [Akasofu, 1981; Baker et al., 1997; Lu et al., 1998] compared to the more conservative value $(2.7 \cdot 10^4)$ suggested by Prigancova and Feldstein [1992].

The average value found for $W(U_J)$ is 56% which may be a lower estimate as the stations used to calculate the AE index were not well located (in longitude) for 2 of the substorms (see Table 1). Another source of underestimation is that during strong events (AE >1000 nT) such as the one on July 31, the electrojets may move equatorward (latitudinal shift) of the stations and thus will be poorly detected. The average value of $W(U_J)$ for the substorms is $2.7 \cdot 10^{15}$ J, which is more than 2.5 times the statistical results for isolated substorms (IS) (see Table 3) which means that these are rather intense substorms.

We have also calculated $W(U_A)$ for each substorm, which was found to vary from $6.6 - 24.0 \cdot 10^{14}$ J, with a mean of $1.35 \cdot 10^{15}$ J. This is an order of magnitude larger than suggested by Akasofu [1981] ($1.4\ 10^{14}$J). Part of this may be that our substorms are more intense than the substorms Akasofu [1981] examined, but maybe more importantly; the parameterized method he used to estimate U_A only gives 1/3 of the U_A [Østgaard et al., 2002 B, in press]. On average the $W(U_A)$ is ~29% of the total energy dissipation, $W(U_T)$. This should be considered as a lower estimate as the integration times used for $W(U_A)$ are shorter than for the other energies.

The ratio of $W(U_J)$ to $W(U_A)$ was found to be ~2. Other studies have reported different values for the ratio, varying from 1.3 [Prigancova and Feldstein, 1992] to 4 [Lu et al., 1995]. However, as discussed by Østgaard et al. [2002 A, in press] these variations can be explained by either calculation inaccuracies [Prigancova and Feldstein, 1992] or significant underestimation of U_A due to limitations in the data used for the estimate [Richmond, 1990; Lu et al., 1995]. Our results are similar to the ratio found by Lu et al. [1998], who used the AMIE procedure, supported by global UVI data to obtain U_J and U_A. The ratios from Knipp et al. [1998] (2.6) and Emery et al. [1999] (2.9) are higher than ours and may be explained by an underestimation of U_A as

they do not take into account electrons with energies > 20 keV.

Comparing $W(\epsilon)$ and $W(U_T)$ we see that the ϵ-parameter does not always provide enough energy to balance U_T, which is similar to what Knipp et al. [1998] found. As Akasofu [1981] originally considered the ionosphere as a minor energy sink, this naturally leads to an underestimation of ϵ when more accurate estimates of U_J and U_A are taken into account [Pulkkinen and Baker, 1997]. However, for the July 24 substorms $W(U_T)$ is a factor of 2 larger than $W(\epsilon)$. One might argue that the magnetosphere stores energy from the solar wind and that energy balance only can be required over long time scales, but for the July 24 events it should be noticed that the energy transfer estimated by ϵ during the two substorms is remarkably low, while the $W(U_{SW})$ is large and the $W(U_T)$ is in the same range as the other substorms (Table 2). Even integration of the ϵ-parameter from an earlier time does not alter this, because another substorm at 0800 - 1100 UT probably dissipated most of the solar wind energy transferred before and during that event. In Figure 5 (from Østgaard et al. [2002 A, in press]) we show the time-integrated total energy balance between energy input and output as a function of time

Figure 5

$$W(t) = \int_{t_1}^{t} \epsilon(t) - U_T(t)dt \qquad (10)$$

As can be seen from the two upper panels and the bottom panel the ϵ-parameter (dashed line) does not provide enough energy to balance U_T. The overall negative slope of $W(t)$ either indicates that that there has to be some other energy transfer mechanism than day-side reconnection, or that the merging area, l_0^2, in the ϵ-function (see, Eq.1) should be increased, or simply that the magnetosphere is dissipating energy stored much earlier. For the July 24 events the merging area, l_0^2, has to be increased by a factor of 2 to balance the $W(U_T)$. Alternatively, if we allow for solar wind energy to be transferred during northward IMF by viscous interaction (U_{VI}), we find that only $U_{VI} = 0.0017\ U_{SW}$ has to be added to the ϵ term to balance the energy budget for the July 24 substorms. The solid line shows the result of calculating

$$W(t) = \int_{t_1}^{t} \epsilon(t) + 0.0017\ U_{SW} - U_T(t)dt \qquad (11)$$

For the July 24 events the energy contribution by $W(U_{VI})$ is similar to $W(\epsilon)$, while $W(U_{VI})$ only adds 10 -20 % of $W(\epsilon)$ for the other events. In Figure 5

increasing $W(t)$ (solid line) indicates the loading of energy (L) during substorm growth phase and decreasing $W(t)$ indicates the energy dissipation (U, for unloading) from substorm onset through the expansion phase. Onset times were determined from global UV and X-ray imaging. Efforts have been made to quantify the viscous energy transfer efficiency, σ_v. By calculating the U_T during 11 intense northward IMF events that lasted for several hours, where the merging of field lines is almost negligible and hence ϵ would be close to zero, Tsurutani and Gonzalez [1995] found that the transfer efficiency, σ_v, had to be 0.001 - 0.004 to balance the energy budget. It should be noticed that this study used the very conservative values from Akasofu [1981] to estimate the U_J and U_A, which means that their σ_v should be closer to 0.003-0.012 rather than 0.001-0.004 if more up-date estimates are used. Our suggestion of $\sigma_v = 0.0017$ is therefore in the low side of the σ_v reported by Tsurutani and Gonzalez [1995].

For the July 31 event there is more energy transferred into the magnetosphere than dissipated during the substorm, indicating that there are energy sinks that were not considered. Such energy sinks might be the plasma sheet heating, which Lu et al. [1998] during a magnetic cloud event estimated to be ~100 GW and in the same range as the U_A or the ejection of plasmoids down the tail, which Ieda et al. [1998] estimated to be roughly 10^{15} J in the course of a substorm. However, for the July 31 event including both these energy sinks is still not sufficient to dissipate the stored energy, which means that there may be a net energy gain in the magnetosphere during this event.

5.2. Statistical results for isolated and stormtime substorms

Energetics of substorms have been studied since 1980's [Akasofu, 1981]. In most studies substorms have been dealt with as a homogeneous group of events. However, there have been suggestions that isolated and stormtime substorms would be different from each other. The results of Baumjohann et al. [1996] seem to show that isolated substorms (which they called non-storm substorms) and stormtime substorms behave differently. Hsu and McPherron [2000] concluded that both classes of substorms are caused by the same mechanism. Nevertheless, they found some differences between two classes of events, which were in absolute values and changes of magnitude; the stormtime substorms were larger than isolated substorms. This is consistent with our results showing that on average stormtime substorms (-665 nT)

are about twice as intense as isolated substorms (-347 nT).

The intensity of a substorm, measured as a minimum of the IL index, has shown to be a good parameter for measuring the substorm size, but it is not by all means a perfect parameter. This is partly because the auroral electrojet indices are recording both external variations, arising from currents in the ionosphere and magnetosphere, and internal variations, arising from the currents induced in the solid Earth [Viljanen et al., 1995]. Internal part of the IL (and AL) is largest for the rapid time variations, such as substorm onset, when the internal part can be as high as 40% of the IL index [Tanskanen et al., 2001]. Internal contribution decreases during expansion and recovery phases to an average of about 15 –20% during non-disturbed times [Tanskanen et al., 2001]. Thus, besides using maximal negative variation of IL index as a measure of substorm size, the integrated IL index, $W(U_J)$, can be used.

$W(U_J)$ during SS is typically two times larger ($1.8 \cdot 10^{15}$ J) than $W(U_J)$ during IS ($0.8 \cdot 10^{15}$ J). However, due to the much larger portion of isolated events the total two-year Joule dissipation was much larger for IS ($7.8 \cdot 10^{17}$ J) than for SS ($3.4 \cdot 10^{17}$ J). This indicates that isolated substorms have a more important role in magnetospheric energetics than previously assumed.

The main difference between IS and SS, besides the differences in IL intensity and $W(U_J)$, is the occurrence frequency. The frequency of IS (SS) was computed by dividing the total number of isolated (stormtime) events by the total period of time when the $Dst > -40$ nT ($Dst < -40$ nT). It was found that isolated substorms occurred every ten hours while stormtime substorms occurred every four hours. This method of computing frequencies includes all the moments of the time, regardless of the solar wind conditions and therefore does not provide a consistent comparison between the two classes of substorms. There were several long periods (several days) in the data where no substorms occurred. If we only include moments of the time when the solar wind conditions were favorable to substorm activity, the frequency of isolated substorms would be much larger, even near the frequency of stormtime substorms. Borovsky et al. [1993] examined substorms, which occurred during favorable solar wind conditions, meaning that the $IMF\ B_Z$ was southward for an extended period of time. They found the average occurrence frequency of substorms to be 5.74 hours with a significant peak at 2-4 hours. The parameter they studied is comparable to the duration of substorm in our statistics,

which was about four hours on average showing a broad peak at 2-5 hours.

Joule heating typically accounts for 50 - 60% of the total energy input when all substorms are considered. Our data indicate that $W(U_J)$ is slightly lower for ISs than for SSs, which may be due to the larger role of the ring current increase during storm times. Besides of many differences between isolated and stormtime substorms there were also some similarities; for example durations and times of the substorm onsets were quite identical for both classes of substorms. Figure 6 shows a cartoon of typical isolated and stormtime substorms. The figure clearly shows that isolated and stormtime substorms are different from each other, but it is still left an open question whether they can be produced by the same mechanisms.

Figure 6

6. CONCLUSIONS

In this paper we have given a presentation of the energy sources and sinks in the SMI system and discussed how well the different forms of energy can be estimated. We have presented results from detailed energy budget analysis of 7 isolated substorms as well as statistical results based on 698 isolated and 141 stormtime substorms. The main results are:

(1) During the 7 isolated substorms the coupling efficiency defined as $W(U_T)/W(U_{SW})$ was found to be 0.3 - 0.8%, which is in reasonable agreement with the results reported by others [Stern, 1984; Knipp et al., 1998; Lu et al., 1995].

(2) For some events the ϵ-parameter does not provide enough energy into the magnetosphere to balance U_T. If we allow for viscous interaction between the solar wind and the magnetosphere, this mechanism only need to transfer 0.17% of U_{SW} to balance the energy budget. This energy transfer would usually represent only a small fraction (10-20%) of what is estimated from the ϵ parameter, but may become important when IMF is northward and $W(U_T)$ is still large. A viscous interaction efficiency of 0.17% is in the low side of what was found by Tsurutani and Gonzalez [1995] .

(3) Examining 7 isolated substorm the energy transferred from the solar wind to the MI system was distributed with an average of 15% to $W(U_R)$, 56% to $W(U_J)$ and 29% to $W(U_A)$, which is close to what was reported by Knipp et al. [1998] during a severe magnetic storm. This distribution of energy is further supported by the statistical results from 698 isolated and 141 stormtime substorms where $W(U_J)$ was found to be slightly less than two thirds of $W(\epsilon)$ during isolated

substorms and about half during stormtimes. Although this result emphasizes that the ring current increase is more important during storm times, $W(U_J)$ is the dominant energy sink during both isolated and stormtime substorms. For the 7 isolated substorms $W(U_A)$ was found to be 1/2 of $W(U_J)$ and in fairly good agreement with magnetic cloud and storm studies [Lu et al., 1998; Knipp et al., 1998]. Most energy budget analyses have underestimated the contribution from U_A, as the input data have not covered the entire energy range of precipitating electrons important to calculate U_A.

(4) Stormtime (isolated) substorms appear in every four (ten) hours, when all solar wind conditions were taken into account. If we would examine only moments of time when the solar wind is favorable to substorm occurrence, then the frequency of isolated substorms would be higher.

(5) Isolated substorms are five times as numerous, but half as intense as stormtime substorms. However, over a 2-year period two times more energy is dissipated through Joule heating during isolated substorm ($7.8 \cdot 10^{17}$ J) than during stormtime substorms ($3.4 \cdot 10^{17}$ J). This indicates that the isolated substorm are the main process by which the solar wind energy is carried to the MI energy sinks.

Acknowledgments.

The authors wish to thank Richard Vondrak and Tuija Pulkkinen for their valuable comments. We thank R. Lepping for the WIND magnetic field data, A. Lazarus for the WIND solar wind data, C. Smith for the ACE magnetic field data and D. McComas doe the ACE solar wind data. We acknowledge the World Data Center for Geomagnetism (T. Kamei), Kyoto, Japan for providing the preliminary Quick look AE, AL and AU indices, and all the institutes maintaining the IMAGE magnetometer network. The work of E.T. was supported by the Academy of Finland and the work of N.Ø. by the Norwegian Research Council.

N.Ø thanks the staff of the NASA/GSFC Laboratory for Extraterrestrial Physics for their hospitality and support during his stay from June 2000 to September 2001. He also wants to thank the PIXIE and UVI teams for useful collaboration.

REFERENCES

Ahn, B. H., S.-I. Akasofu, and Y. Kamide, The Joule heat production rate and the particle energy injection rate as a function of the geomagnetic indices AE and AL , *J. Geophys. Res.*, *88*, 6275–6287, 1983.

Ahn, B. H., H. W. Kroehl, Y. Kamide, and D. J. Gorney, Estimation of ionospheric electrodynamic prameters using

ionospheric conductance deduced from Bremsstrahlung X-ray image data, *J. Geophys. Res.*, *94*, 2565–2586, 1989.

Akasofu, S.-I., The development of the auroral substorm, *Planet. Space Sci.*, *12*, 273–282, 1964.

Akasofu, S.-I., Energy coupling between the solar wind and the magnetosphere, *Space Sci. Rev.*, *28*, 121–190, 1981.

Allen, J. H., and H. W. Kroehl, Spatial and temporal distributions of magnetic effects of auroral electrojets as derived from *AE* indices, *J. Geophys. Res.*, *80*, 3667–3677, 1975.

Axford, W. I., and C. O. Hines, A unifying theory of high-latitude geophysical phenomena and geomagnetic storms, *Canadian J. Phys.*, *39*, 1433–1464, 1961.

Baker, D. N., S.-I. Akasofu, W. Baumjohann, J. W. Bieber, D. M. Fairfield, E. W. Hones, B. Mauk, R. L. McPherron, and T. E. Moore, Substorms in the magnetosphere, *NASA Ref. Publ., 1120*, 1984.

Baker, D. N., T. I. Pulkkinen, M. Hesse, and R. L. McPherron, A quantitative assessment of energy storage and release in the Earth's magnetotail, *J. Geophys. Res.*, *102*, 7159–7168, 1997.

Baker, D. N., S. G. Kanekal, J. B. Blake, and T. I. Pulkkinen, The global efficiency of relativistic electron production in the Earth's magnetosphere, *J. Geophys. Res.*, *106*, 19,169–19,178, 2001.

Bargatze, L. F., D. N. Baker, R. L. McPherron, and E. W. Hones, Jr., Magnetospheric impulse response for many levels of geomagnetic activity, *J. Geophys. Res.*, *90*, 6387–6394, 1985.

Baumjohann, W., and Y. Kamide, Hemispherical Joule heating and the AE indices, *J. Geophys. Res.*, *89*, 383–388, 1984.

Baumjohann, W., Y. Kamide, and R. Nakamura, Substorms, storms and the near-Earth tail, *J. Geomagn. Geoelectr.*, *48*, 177–185, 1996.

Borovsky, J. E., R. J. Nemzek, and R. D. Belian, The occurrence rate of magnetospheric substorm onsets: Random and periodic substorms, *J. Geophys. Res.*, *98*, 3807–3813, 1993.

Caan, M. N., R. L. McPherron, and C. T. Russell, The statistical magnetic signature of magnetospheric substorms, *Planet. Space Sci.*, *26*, 269, 1978.

Codrescu, M. V., T. J. Fuller-Rowell, and J. C. Foster, On the importance of E-field variability for Joule heating in the high-latitude thermosphere, *Geophys. Res. Lett.*, *22*, 2393–2396, 1995.

Collier, M. R., J. A. Slavin, R. P. Lepping, A. Szabo, and K. Ogilvie, Timing accuracy for the simple planar propgation magnetic field structures in the solar wind, *Geophys. Res. Lett.*, *25*, 2509–2512, 1998.

Cooper, M. L., C. R. Clauer, B. A. Emery, A. D. Richmond, and J. D. Winningham, A storm time assimilative mapping of ionospheric electrodynamics analysis for the

severe geomagnetic storm of November 8-9, 1991, *J. Geophys. Res.*, *100*, 19,329–19,342, 1995.

Elphinstone, R. D., J. S. Murphree, and L. L. Cogger, What is a global auroral substorm?, *Rev. Geophys.*, *34*, 169–232, 1996.

Emery, B. A., C. Lathuillere, P. G. Richards, R. G. Roble, M. J. Buonsanto, D. J. Knipp, P. Wilkinson, D. P. Sipler, and R. Niciejewski, Time dependent thermospheric neutral response to the 2-11 November 1993 storm period, *J. Atmos. Terr. Phys.*, *61*, 329–350, 1999.

Farrugia, C. J., F. T. Gratton, and R. B. Torbert, Viscous-type processes in the solar wind-magnetosphere interaction, *Space Sci. Rev.*, *95*, 443–456, 2001.

Germany, G. A., G. K. Parks, M. Brittnacher, J. Cumnock, D. Lummerzheim, J. F. Spann, L. Chen, P. G. Richards, and F. J. Rich, Remote determination of auroral energy characteristics during substorm activity, *Geophys. Res. Lett.*, *24*, 995, 1997.

Germany, G. A., G. K. Parks, M. J. Brittnacher, J. F. Spann, J. Cumnock, D. Lummerzheim, F. Rich, and F. G. Richards, Energy characterization of a dynamic auroral event using GGS UVI images, in *Geospace Mass and Energy Flow: Results From the International Solar-Terrestrial Physic Program, Geophys. Monogr. Ser.,* vol. 104, edited by J. L. Horwitz, D. L. Gallagher, and W. K. Peterson, p. 143, AGU, Washington, D. C., 1998a.

Germany, G. A., J. F. Spann, G. K. Parks, M. J. Brittnacher, R. Elsen, L. Chen, D. Lummerzheim, and M. H. Rees, Auroral observations from the POLAR Ultraviolet Imager (UVI), in *Geospace Mass and Energy Flow: Results From the International Solar-Terrestrial Physic Program, Geophys. Monogr. Ser.,* vol. 104, edited by J. L. Horwitz, D. L. Gallagher, and W. K. Peterson, p. 149, AGU, Washington, D. C., 1998b.

Gonzalez, W. D., J. A. Joselyn, Y. Kamide, H. W. Kroehl, G. Rostoker, B. T. Tsurutani, and V. M. Vasyliunas, What is a geomagnetic storm?, *J. Geophys. Res.*, *99*, 5771–5792, 1994.

Holzer, R. E., and J. A. Slavin, En evaluation of three predictors of geomagnetic activity, *J. Geophys. Res.*, *87*, 2558, 1982.

Hsu, T.-S., and R. McPherron, The characteristics of storm-time substorms and non-storm substorms, in *Proceedings of ICS-5, Fifth international conference on substorms, ESA SSP-443*, edited by A. Wilson, pp. 439–442, ESA-ESTEC, Noordwijk, Netherlands, 2000.

Ieda, A., S. Machida, T. Mukai, Y. Saito, T. Yamamoto, A. Nishida, T. Terasawa, and S. Kokubun, Statistical analysis of the plasmoid evolution with Geotail observations, *J. Geophys. Res.*, *103*, 4453–4465, 1998.

Imhof, W. L., et al., The Polar Ionospheric X-ray Imaging Experiment (PIXIE), *Space Sci. Rev.*, *71*, 385–408, 1995.

Kallio, E. I., T. I. Pulkkinen, H. E. J. Koskinen, A. Viljanen, J. A. Slavin, and K. Ogilvie, Loading-unloading processes

in the nightside ionosphere, *Geophys. Res. Lett.*, *27*, 1627–1630, 2000.

Kamide, Y., and S.-I. Akasofu, Notes on the auroral electrojet indices, *Rev. Geophys. Space Phys.*, *21*, 1647–1656, 1983.

Kan, J. R., L. Zhu, A. T. Y. Lui, and S.-I. Akasofu, A magnetosphere-ionosphere coupling theory of substorms including magnetotail dynamics, in *Auroral Physics*, edited by C.-L. Meng, M. J. Rycroft, and L. A. Frank, pp. 311–321, Cambridge Univ. Press, New York, 1991.

Kauristie, K., T. I. Pulkkinen, R. J. Pellinen, and H. J. Opgenoorth, What can we tell about auroral electrojet activity from a single meridional magnetometer chain, *Ann. Geophys.*, *14*, 1177–1185, 1996.

Knipp, D. J., et al., An overview of the early November 1993 geomagnetic storm, *J. Geophys. Res.*, *103*, 26,197–26,220, 1998.

Lepping, R. P., et al., The WIND magnetic field investigation, *Space Sci. Rev.*, *71*, 207–229, 1995.

Liou, K., P. T. Newell, C. I. Meng, M. Brittnacher, and G. Parks, Characteristics of the solar wind controlled auroral emissions, *J. Geophys. Res.*, *103*, 17,543–17,557, 1998.

Lu, G., D. Richmond, B. A. Emery, and R. G. Roble, Magnetosphere-ionosphere-thermosphere coupling: Effect of neutral winds on energy transfer and field-aligned current, *J. Geophys. Res.*, *100*, 19,643–19,659, 1995.

Lu, G., et al., Global energy deposition during the January 1997 magnetic cloud event, *J. Geophys. Res.*, *103*, 11,685–11,694, 1998.

McComas, D. J., S. J. Bame, P. Barker, W. Feldman, J. L. Phillips, P. Riley, and J. W. Griffee, Solar wind electron proton alpha monitor (SWEPAM) for the advanced composition explorer, *Space Sci. Rev.*, *86*, 563, 1998.

Nisbet, J. S., Relations between the Birkeland currents, the auroral electrojet indices and high latitude Joule heating, *J. Atmos. Terr. Phys.*, *44*, 797–809, 1982.

Ogilvie, K. W., et al., SWE, A comprehensive plasma instrument for the WIND spacecraft, *Space Sci. Rev.*, *71*, 55–77, 1995.

Østgaard, N., J. Stadsnes, J. Bjordal, R. R. Vondrak, S. A. Cummer, D. Chenette, M. Schulz, and J. Pronko, Cause of the localized maximum of X-ray emission in the morning sector: A comparison with electron measurements, *J. Geophys. Res.*, *105*, 20,869, 2000.

Østgaard, N., J. Stadsnes, J. Bjordal, G. A. Germany, G. K. Parks, R. R. Vondrak, S. A. Cummer, D. Chenette, and J. Pronko, Auroral electron distributions derived from combined UV and X-ray emissions, *J. Geophys. Res.*, *106*, 26,081–26,090, 2001.

Østgaard, N., G. A. Germany, J. Stadsnes, and R. R. Vondrak, Energy analysis of substorms based on remote sensing techniques, solar wind measurements and geomagnetic indices, *J. Geophys. Res.*, –, –, 2002 A, in press.

Østgaard, N., R. R. Vondrak, J. W. Gjerloev, and G. A. Germany, A relation between the energy deposition by electron precipitation and geomagnetic indices during substorms, *J. Geophys. Res.*, –, –, 2002 B, in press.

Parks, G. K., *Physics of space plasmas*, The Advanced Book Program, 1 ed., Addison-Wesley Publishing Company, 350 Bridge Parkway, Redwood City, CA 94065, 1991.

Perrault, P., and S. I. Akasofu, A study of magnetic storms, *Geophys. J. R. Astrom. Soc.*, *54*, 547–573, 1978.

Prigancova, A., and Y. I. Feldstein, Magnetospheric storm dynamics in terms of energy output rate, *Planet. Space Sci.*, *40*, 581–588, 1992.

Pulkkinen, T. I., and D. N. Baker, Global substorm cycle: What can the models tell us?, in *Surveys in Geophysics*, vol. 18, pp. 1–37, Kluwer Academic Publishers, 1997.

Richmond, A. D., Global measures of ionospheric electrodynamic activity inferred from combined incoherent scatter radar and ground magnetometer observations, *J. Geophys. Res.*, *95*, 1061, 1990.

Rostoker, G., Overviw of observations and models of auroral substorms, in *Auroral Physics*, edited by C.-L. Meng, M. J. Rycroft, and L. A. Frank, pp. 257–272, Cambridge University Press, New York, 1991.

Rostoker, G., J. C. Samson, F. Creutzberg, T. J. Hughes, D. R. McDiarmid, A. G. McNamara, A. Vallance-Jones, D. D. Wallis, and L. L. Cogger, CANOPUS - a ground based instrument array for remote sensing the high latitude ionosphere during the ISTP/GGS program, *Space Sci. Rev.*, *71*, 743–760, 1995.

Russell, C. T., and R. L. McPherron, The magnetotail and substorms, *Space Sci. Rev.*, *15*, 205–266, 1973.

Shue, J. H., J. K. Chao, H. C. Fu, C. T. Russell, P. Song, K. K. Khurana, and H. J. Singer, A new functional form to study the solar wind control of the magnetopause size and shape, *J. Geophys. Res.*, *102*, 9497–9511, 1997.

Shue, J.-H., et al., Magnetopause location under extreme solar wind conditions, *J. Geophys. Res.*, *103*, 17,691–17,700, 1998.

Smith, C. W., J. L'Heureux, N. F. Ness, M. Acuña, L. F. Burlaga, and J. Scheifele, The ACE magnetic fields experiments, *Space Sci. Rev.*, *86*, 613, 1998.

Spiro, R. W., D. H. Reiff, and J. L. J. Mather, Precipitating electron average flux and auroral zone conductance. An empirical model, *J. Geophys. Res.*, *87*, 8215, 1982.

Stamper, R., M. Lockwood, M. Wild, and T. D. G. Clark, Solar causes of the long-term increase in geomagnetic activity, *J. Geophys. Res.*, *104*, 18,325, 1999.

Stern, D. P., Energetics of the magnetosphere, *Space Sci. Rev.*, *39*, 193–213, 1984.

Sugiura, M., Hourly values of equatorial Dst for the IGY, in *Annual International Geophysical Year*, vol. 35, p. 9, Pergamon, New York, 1964.

Syrjäsuo, M., et al., Observations of substorm electrodynamics using the MIRACLE network, in *Substorms-4*,

edited by S. Kokubun and Y. Kamide, pp. 111–114, Terra Scientific Publishing Company, Tokyo, 1998.

Tanskanen, E., T. I. Pulkkinen, H. E. J. Koskinen, and J. A. Slavin, Substorm energy budget during low and high solar activity: 1997 and 1999 compared, *J. Geophys. Res.*, *107*, –, 2002.

Tanskanen, E. I., A. Viljanen, T. Pulkkinen, L. H. R. Pirjola, A. Pulkkinen, and O. Amm, At substorm onset, 40% of AL comes from underground, *J. Geophys. Res.*, *106*, 13,119–13,134, 2001.

Torr, M. R., et al., A far ultraviolet imager for the international solar-terrestrial physics mission., *Space Sci. Rev.*, *71*, 329–383, 1995.

Tsurutani, B. T., and W. Gonzalez, The efficiency of "viscous interaction" between the solar wind and the magnetosphere during intense northward IMF events, *Geophys. Res. Lett.*, *22*, 663–666, 1995.

Tsurutani, B. T., J. A. Slavin, Y. Kamide, R. D. Zwickl, J. H. King, and C. T. Russell, Coupling between the solar wind and the magnetosphere: CDAW 6, *J. Geophys. Res.*, *90*, 1191–1199, 1985.

Turner, N. E., D. N. Baker, T. I. Pulkkinen, and G. Lu, Global energy partition during magnetic storms, *J. Geophys. Res.*, 2001, in press.

Valdivia, J. A., A. S. Sharma, and K. Papadopoulos, Prediction of magnetic storms by nonlinear models, *Geophys. Res. Lett.*, *23*, 2899–2902, 1996.

Vassiliadis, D., A. J. Klimas, J. A. Valdivia, and D. N. Baker, The *Dst* geomagnetic response as a function of storm phase and amplitude and the solar wind electric field, *J. Geophys. Res.*, *104*, 24,957–24,976, 1999.

Viljanen, A., K. Kauristie, and K. Pajunpää, On induction effects at EISCAT and IMAGE magnetometer stations, *Geophys. J. Int.*, *121*, 893, 1995.

Weiss, L. A., P. Reiff, J. Moses, R. Heelis, and B. Moore, Energy dissipation in substorms, in *Proceedings of the International Conference on Substorms ICS-1*, vol. ESA SP-335, pp. 309–317, Eur. Space Agency Spec. Publ., 1992.

Zwickl, R. D., L. F. B. D. N. Baker, C. R. Clauer, and R. L. McPherron, An evaluation of the total magnetospheric energy output parameter, U_T, in *Magnetotail Physics*, edited by A. T. Y. Lui, pp. 155–159, Johns Hopkins Univ. Press, Baltimore, Md., 1987.

N. Østgaard, Space Sciences Laboratory, University of California, Centennial Drive at Grizzly Peak Blvd., Berkeley, CA 94720-7450 (e-mail: nikost@ssl.berkeley.edu)

E. Tanskanen, Laboratory for Extraterrestrial Physics, Code 696, Building 2, NASA/GSFC Greenbelt, MD 20771 (e-mail: etanskanen@lepvax.gsfc.nasa.gov)

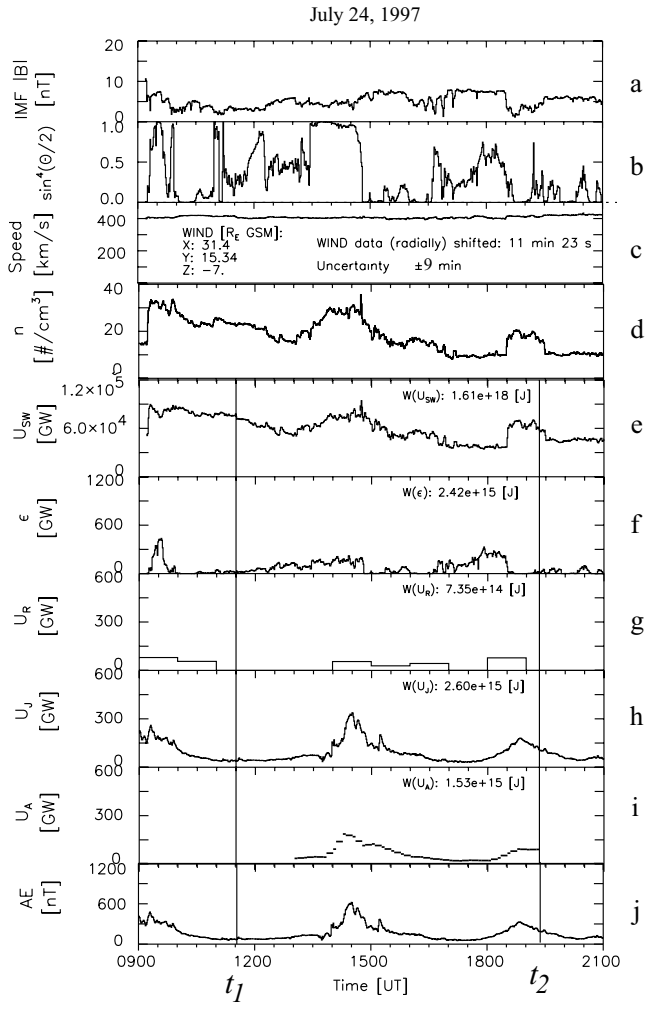

Figure 1. (a-f) Solar wind parameters and energy input measured by WIND. The data are shifted by to the radial distance of the spacecraft and the expected ~5 min propagation time from the subsolar point to the ionosphere [Kan et al., 1991]. (a) The scalar magnitude interplanetary magnetic field. (b) $\sin^4(\frac{\theta_c}{2})$, where θ_c is the clock angle of the interplanetary field. (c) The solar wind bulk speed. (d) Solar wind density. (e) The available solar wind kinetic energy (U_{SW}). (f) ϵ-parameter. (g-i) The various energy dissipations in the MI system. (g) The energy increase of the ring current (U_R). (h) The Joule heating rate in both hemispheres (U_J). (i) The rate of energy deposition by electron precipitation in both hemispheres derived from UV- and X-ray emissions (U_A). (j) The AE quick look index. The solid vertical lines denote the time interval used for integration from t_1 to t_2. The time-integrated energies ($W(U)$) are calculated in panel e-i.

Figure 1. (a-f) Solar wind parameters and energy input measured by WIND. The data are shifted by to the radial distance of the spacecraft and the expected ~5 min propagation time from the subsolar point to the ionosphere [Kan et al., 1991]. (a) The scalar magnitude interplanetary magnetic field. (b) $\sin^4(\frac{\theta_c}{2})$, where θ_c is the clock angle of the interplanetary field. (c) The solar wind bulk speed. (d) Solar wind density. (e) The available solar wind kinetic energy (U_{SW}). (f) ϵ-parameter. (g-i) The various energy dissipations in the MI system. (g) The energy increase of the ring current (U_R). (h) The Joule heating rate in both hemispheres (U_J). (i) The rate of energy deposition by electron precipitation in both hemispheres derived from UV- and X-ray emissions (U_A). (j) The AE quick look index. The solid vertical lines denote the time interval used for integration from t_1 to t_2. The time-integrated energies ($W(U)$) are calculated in panel e-i.

Figure 1. (a-f) Solar wind parameters and energy input measured by WIND. The data are shifted by to the radial distance of the spacecraft and the expected ~5 min propagation time from the subsolar point to the ionosphere [Kan et al., 1991]. (a) The scalar magnitude interplanetary magnetic field. (b) $\sin^4(\frac{\theta_c}{2})$, where θ_c is the clock angle of the interplanetary field. (c) The solar wind bulk speed. (d) Solar wind density. (e) The available solar wind kinetic energy (U_{SW}). (f) ϵ-parameter. (g-i) The various energy dissipations in the MI system. (g) The energy increase of the ring current (U_R). (h) The Joule heating rate in both hemispheres (U_J). (i) The rate of energy deposition by electron precipitation in both hemispheres derived from UV- and X-ray emissions (U_A). (j) The AE quick look index. The solid vertical lines denote the time interval used for integration from t_1 to t_2. The time-integrated energies ($W(U)$) are calculated in panel e-i.

Figure 1. (a-f) Solar wind parameters and energy input measured by WIND. The data are shifted by to the radial distance of the spacecraft and the expected ~5 min propagation time from the subsolar point to the ionosphere [Kan et al., 1991]. (a) The scalar magnitude interplanetary magnetic field. (b) $\sin^4(\frac{\theta_c}{2})$, where θ_c is the clock angle of the interplanetary field. (c) The solar wind bulk speed. (d) Solar wind density. (e) The available solar wind kinetic energy (U_{SW}). (f) ϵ-parameter. (g-i) The various energy dissipations in the MI system. (g) The energy increase of the ring current (U_R). (h) The Joule heating rate in both hemispheres (U_J). (i) The rate of energy deposition by electron precipitation in both hemispheres derived from UV- and X-ray emissions (U_A). (j) The AE quick look index. The solid vertical lines denote the time interval used for integration from t_1 to t_2. The time-integrated energies ($W(U)$) are calculated in panel e-i.

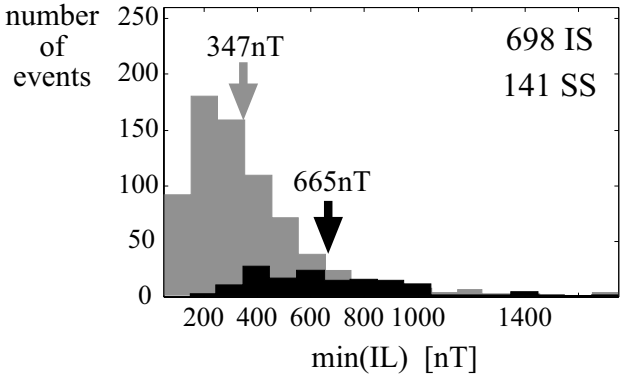

Figure 2. Intensity histograms, binned by every 100 nT, for isolated (IS) and stormtime substorms. Number of the events are marked to the upper right corner.

Figure 2. Intensity histograms, binned by every 100 nT, for isolated (IS) and stormtime substorms. Number of the events are marked to the upper right corner.

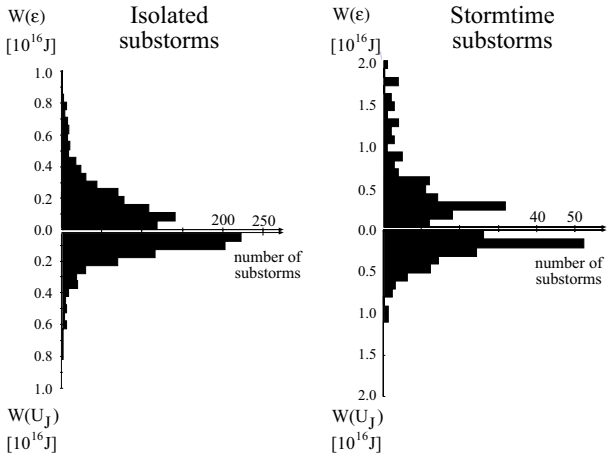

Figure 3. (a) Energy input, $W(\epsilon)$, and two-hemisphere Joule dissipation, $W(U_J)$, histograms for isolated substorms. Both histograms are binned by every $0.5 \cdot 10^{15}$ J. (b) $W(\epsilon)$ and $W(U_J)$ histograms, binned by every 10^{15} J, for stormtime substorms. Note that the scales are different.

Figure 3. (a) Energy input, $W(\epsilon)$, and two-hemisphere Joule dissipation, $W(U_J)$, histograms for isolated substorms. Both histograms are binned by every $0.5 \cdot 10^{15}$ J. (b) $W(\epsilon)$ and $W(U_J)$ histograms, binned by every 10^{15} J, for stormtime substorms. Note that the scales are different.

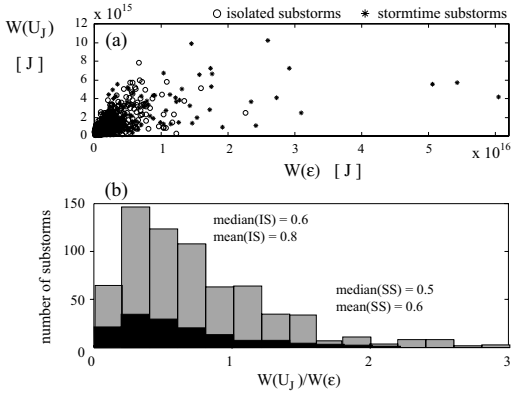

Figure 4. (a) Scatter plot for energy input and two-hemisphere Joule heating. Isolated substorms are marked with circles and stormtime substorms with asterisk. (b) Histograms for input-output ratio, separately for isolated substorms and stormtime substorms. Both means and medians are presented.

Figure 4. (a) Scatter plot for energy input and two-hemisphere Joule heating. Isolated substorms are marked with circles and stormtime substorms with asterisk. (b) Histograms for input-output ratio, separately for isolated substorms and stormtime substorms. Both means and medians are presented.

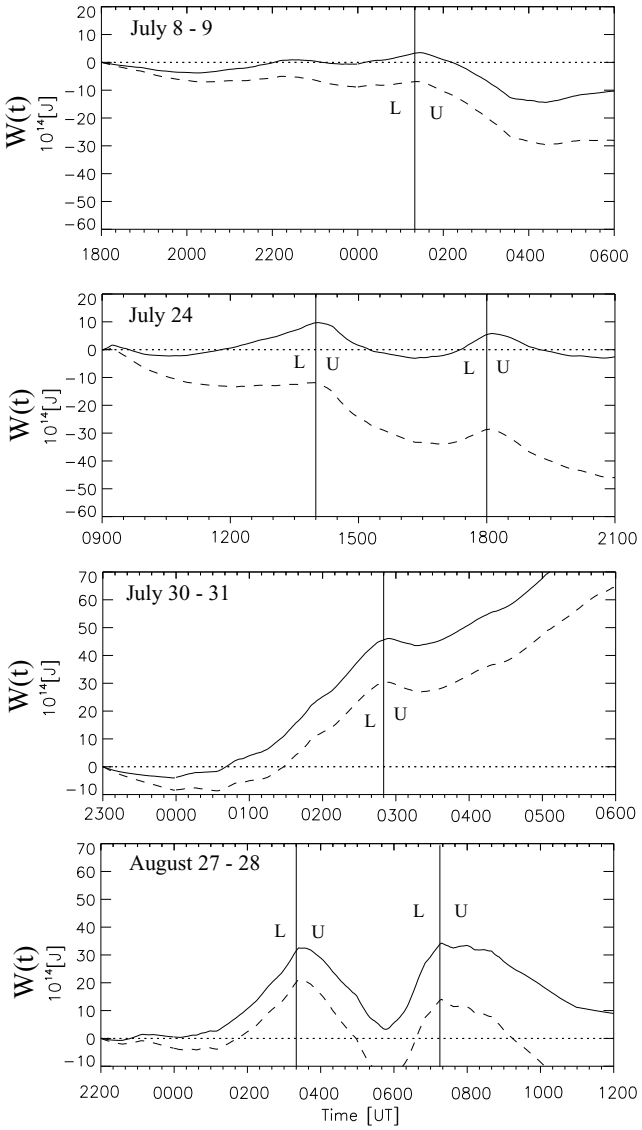

Figure 5. The time-integrated total energy balance between energy input and output ($W(t)$) as a function of time, see Eq. 10. Dashed line: Energy input estimated by ϵ only. Solid line: Energy input is calculated as $\epsilon + 0.0017 U_{SW}$, where U_{SW} is the kinetic solar wind flux given by Eq. 2. We have indicated the times of energy loading (L) and energy unloading (U).

Figure 5. The time-integrated total energy balance between energy input and output ($W(t)$) as a function of time, see Eq. 10. Dashed line: Energy input estimated by ϵ only. Solid line: Energy input is calculated as $\epsilon + 0.0017 U_{SW}$, where U_{SW} is the kinetic solar wind flux given by Eq. 2. We have indicated the times of energy loading (L) and energy unloading (U).

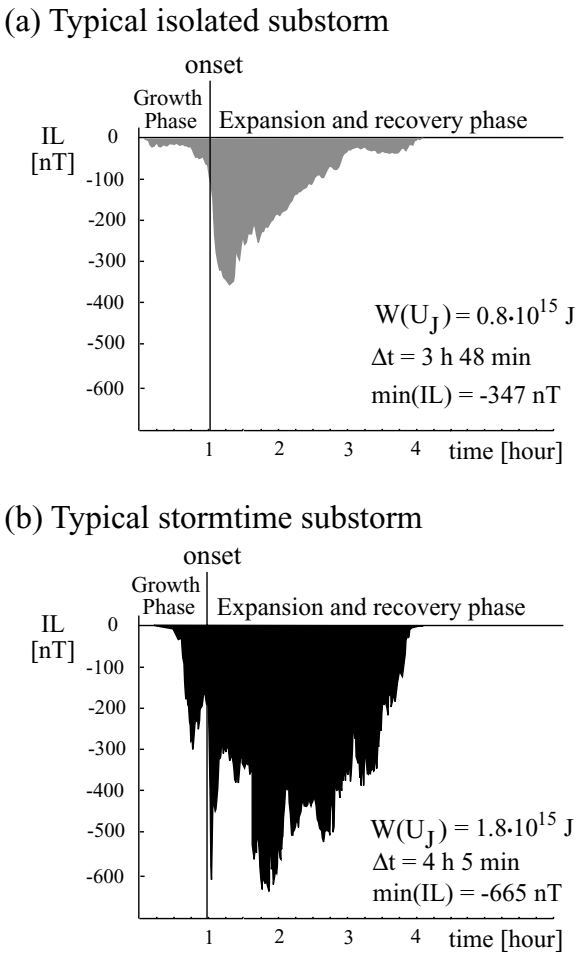

Figure 6. A cartoon of (a) typical isolated substorm and (b) typical stormtime substorm.

Figure 6. A cartoon of (a) typical isolated substorm and (b) typical stormtime substorm.

Table 1. Onset times and geomagnetic conditions for the 7 substorms

Table 1. Onset times and geomagnetic conditions for the 7 substorms

Date	Onset	Dst	Kp	AE max
1) 970709	0120	−9	3−	600
2) 970709[a]	0400	−17	3−	250
3) 970724	1400	12	4−	600
4) 970724	1830	8	3−	300
5) 970731[a]	0240	−20	4+	1100
6) 970828	0245	−6	2+	900
7) 970828	0600	−48	4+	500

[a] The stations used to calculate AE_{QL}, AU_{QL} and AL_{QL} are not well located regarding the regions of intense electron precipitation.

Table 2. Total energy budget for seven selected substorms

Table 2. Total energy budget for seven selected substorms

Date	#[a]	$W(U_R)$	$W(U_J)$[b]	$W(U_A)$[b]	$W(U_T)$[c]	$W(\epsilon)$	$W(U_{SW})$	CE[d]
(hours)[e]		$[10^{14}\mathrm{J}]$ (%)[f]	$[10^{14}\mathrm{J}](\%)$[f]	$[10^{14}\mathrm{J}](\%)$[f]	$[10^{14}\mathrm{J}]$	$[10^{14}\mathrm{J}]$	$[10^{16}\mathrm{J}]$	[%]
970709 (8.5-4)	2	3.8 (6)	42.2 (69)	15.1 (25)	61.1	47.0	78.5	0.8
970724 (7.8-6.3)	2	7.4 (15)	26.0 (53)	15.3 (32)	48.7	24.2	161.0	0.3
970731 (3.7-2.3)	1	4.6 (11)	23.2 (56)	13.5 (33)	41.3	83.3	78.8	0.5
970828 (10.8-8.3)	2	36.8 (26)	61.4 (44)	41.0 (30)	139.2	135.0	152.0	0.8
Average		(15)	(56)	(29)				

[a] Number of substorms

[b] Both hemispheres

[c] $W(U_T) = W(U_R) + W(U_J) + W(U_A)$

[d] CE: Coupling Efficiency defined as $W(U_T)/W(U_{SW})$

[e] Hours of integration for: $W(U_R), W(U_J), W(\epsilon)$ - and : $W(U_A)$

[f] % of $W(U_T)$

Table 3. Comparison of isolated (IS) and stormtime substorms (SS) in terms of energies.

Table 3. Comparison of isolated (IS) and stormtime substorms (SS) in terms of energies.

	$W(U_J)^a$ $[10^{15}$ J] mean	$W(U_J)^b$ $[10^{15}$ J] median	$(\frac{W(U_J)}{W(\epsilon)})^c$ [%] median	$\sum W(U_J)^d$ $[10^{17}$ J]
all	1.3	0.9	60	11.2
IS	1.1	0.8	61	7.8
SS	2.4	1.8	48	3.4

[a] Average of $W(U_J)$

[b] Typical $W(U_J)$, median

[c] Median of ratio $W(U_J)/W(\epsilon)$

[d] Total Joule dissipation during two years under study, $\sum W(U_J)$

Table 4. Comparison of IS and SS.

Table 4. Comparison of IS and SS.

	n[a]	Δt[b]	f[c] [1/h]	t_o[d] [MLT]	$min(IL)$[e] [nT]
all	839	3h 50 min	1/9	22:50	−400
IS	698	3h 47 min	1/10	23:01	−347
SS	141	4h 5 min	1/4	22:14	−665

[a] Number of substorms

[b] Duration of substorms

[c] Occurrence frequency

[d] Magnetic local time of substorm onset

[e] The minimum of the IL index